



## Performance of Under Shear Reinforced Concrete Beams with varying Strength against Static and Impact Load

K Senthil<sup>a1</sup> and Manish Khanna<sup>b</sup>,

<sup>a</sup>Assistant Professor, Department of Civil Engineering, Dr. B R Ambedkar National Institute of Technology, Jalandhar, Punjab, India – 144008

<sup>b</sup>Research Scholar, Department of Civil Engineering, Dr. B R Ambedkar National Institute of Technology, Jalandhar, Punjab, India – 144008

Received: 30/07/2024

Revised: 14/10/2024

Accepted: 08/11/2024

### Abstract

An attempt has been made to study the response of under shear reinforced concrete (RC) beams with varying strength concrete under static and impact load. The experiment has been performed on beam strength as 20, 30, 40 and 50 MPa having cross sections of 50 x 100 mm with a span of 1.1 m. Also, a benchmark study was performed under four-point bending static test and further, three-point bending were converted theoretically in order to keep the test configuration equivalent to three-point impact load test for the comparison. The resistance of reinforced concrete beams was studied in terms of impact force versus time and the deformed profile. It was observed that the resistance of beams was found to increase with increasing the strength of concrete; however, the beams were failed by shear, the reason may be due to the lack of shear capacity. The peak static force by four point bending tests found to be 33% higher than three point bending tests. It was also observed that the dynamic amplification factor (DAF) increases with increase of concrete strength and highest DAF found to be 4.75 corresponding M50 concrete whereas the same was found to be 3.5 corresponding M20 concrete.

<sup>1</sup> Corresponding Author: Dr. K. Senthil

Email: [kasilingams@nitj.ac.in](mailto:kasilingams@nitj.ac.in); [urssenthil85@yahoo.co.in](mailto:urssenthil85@yahoo.co.in); [urssenthil85@gmail.com](mailto:urssenthil85@gmail.com)  
Phone: +91-8267927382, Tel: +91-181-5037555, Fax: +91-181-2690301

**Keywords:** Under shear reinforced concrete beam; Static loading; Impact loading; Dynamic Increase Factor; Deformation Capacity.

## 1. Introduction

Among all the building materials used around the world, concrete is a cost-effective building material. Concrete is also known to be the widely used building material because of its durability. However, concrete also has some unfavourable features and the brittle behaviour of concrete makes it unsuitable to be used as a tension bearing member. It is strong in compression but weak in tension and has low deformation capacity. A lot of research has been observed in this field so as to obtain the concrete which can give us the desirable outputs. To derive a material having greater tensile strength, better resilience, improved ductility and to arrest the propagation of cracks through the concrete matrix, various tests have been performed in the past. In 1987, **Banthia et al.** investigated the effects of a 345 kg mass impact load on simply supported beams that were 1400 mm long and 100 x 125 mm in cross-section. It was determined that the greater internal microcracking is most likely the cause of the higher fracture energy measured in the case of concrete at a higher stress rate. Additionally, it was shown that the ductility and enhanced impact resistance of fiber-reinforced concrete make it superior to plain concrete in dynamic settings. **Fujikake et al. (2009)** concluded that the failure mode of RC beams was significantly affected with the variation of the amount of longitudinally placed steel reinforcement. When small amount of longitudinal steel reinforcement provided, the RC beam exhibited overall flexural failure. Whereas overall flexural failure as well as local failure taking place near impact loading point under the influence of large impact on a single point when comparatively higher amount of longitudinal reinforcement was provided. **Bhatti et al. (2011)** conducted experimental and numerical analyses on reinforced concrete arch beams subjected to impact loading. Their findings showed that the maximum mid-span displacement time history from the numerical simulation aligned well with the experimental results; however, the residual displacement from the simulations was approximately 1.5 to 2.0 times higher than the experimental values.

**Saifullah et al. (2011)** concluded that the ultimate load-carrying capacity of plain concrete is 0.14 times that of under-reinforced concrete beams. In under-reinforced beams, more elements reached their ultimate stress compared to over-reinforced beams. Among the experimentally studied reinforcement ratios, the under-reinforced ratio was identified as optimal, offering the greatest warning zone before failure. It was also observed that

reinforcement in under-reinforced sections reached ultimate stress, whereas in over-reinforced sections, the reinforcement reached only 87% of the ultimate stress. **Zhou et al. (2011)** proposed a “concurrent flexural strength and deformability design” method, enabling simultaneous consideration of strength and deformability requirements. This approach provides engineers flexibility to use high-strength concrete, incorporate compression steel, or add confinement to enhance the deformability of reinforced concrete beams. **Wu et al. (2014)** reported that the capacity increase factor ranged from 1.5 to 8 for load velocities between 30 MN/s and 500 MN/s, while the dynamic increase factor ranged from 1.5 to 3.5 for strain rates between 0.2 and 4 s<sup>-1</sup>. They also observed that the hammer-pad-transducer system consumed nearly half of the energy due to plastic deformation and inertia. The aluminum-alloy pad irreversibly absorbed plastic energy, whereas a rubber-tup loading system consumed more energy during impact. **Anil et al. (2016)** investigated beams made of low-strength concrete, normal-strength concrete, and engineered cementitious composites (ECC) with polyvinyl alcohol (PVA) fibers under dynamic impact loading. The results showed that material type significantly influenced crack width, with the smallest cracks forming in ECC and the largest in low-strength concrete.

**Sindy et al. (2018)** observed that the failure modes and crack patterns of recycled concrete beams were generally similar to those of natural aggregate concrete beams. However, as the replacement rate increased, the cracking moment decreased, and the crack width of recycled concrete beams increased. **Meola et al. (2018)** suggested that infrared thermography could help establish a correlation between impact energy and resulting damage, providing valuable insights for designing new materials. **Wongmatar et al. (2018)** emphasized the importance of maintaining proper stirrup spacing and diameter to prevent failures in reinforced concrete (RC) beams. Specifically, in the impact region, the stirrup spacing and diameter should be at least one-fourth of the effective depth, with a minimum diameter of 6 mm, to avoid brittle shear failure under impact loading. **Soleimani and Roudsari (2019)** studied the effects of impact and quasi-static loading on RC beams, finding that beam stiffness decreased with increasing drop height of the impactor. They also demonstrated that applying glass-fiber-reinforced polymer fabric to the surface of RC beams improved stiffness. Numerical simulations using ABAQUS software showed good agreement with experimental results. **Jin et al. (2020)** investigated the behavior of steel fiber-reinforced concrete (SFRC) beams under multiple impact loads. They observed that mid-span deflection increased with the number of blows, and the crack pattern transitioned from punching shear to bending. Compared to RC beams, SFRC beams exhibited significantly reduced mid-span deflection. Among the

configurations studied, SFRC beams with 2% fiber content and a 0.25% stirrup ratio performed best in terms of energy absorption, dynamic shear capacity, and stability under multiple impacts.

**El-Mandouh et al. (2021)** investigated epoxy-modified reinforced concrete (EMRC) beams, where ordinary Portland cement was partially replaced with epoxy. The study concluded that EMRC beams exhibited reduced deformation, higher shear capacity at both cracking and ultimate levels, and greater displacement ductility compared to conventional concrete beams. Increasing the epoxy content in EMRC beams resulted in less crack propagation, narrower cracks, and more distributed cracking. **Wadhah et al. (2021)** analyzed reinforced concrete beams incorporating granulated blast furnace slag (GBFS) as a cement substitute and recycled block aggregates (RBA). They observed reductions in compressive strength and flexural tensile strength, with extreme reductions of 50% and 55%, respectively, at 70% GBFS and 25% RBA. However, the use of GBFS, RBA, and fibers made the beams more ductile compared to conventional beams. **Anike et al. (2022)** found that incorporating 100% recycled aggregate and 1% steel fiber increased the load-bearing capacity of beams by up to 13% compared to a similar mix without steel fibers and by 8% compared to a reference mix. Notably, a beam with 60% recycled aggregate achieved the same load resistance of 63 kN as the reference beam made entirely of natural aggregate. **Fang et al. (2022)** observed that recycled concrete beams exhibited smaller cracking moments and narrower cracks compared to normal aggregate beams. Increasing the longitudinal reinforcement ratio significantly improved the cracking resistance and flexural capacity of recycled aggregate self-consolidating concrete (RASCC) beams. **Moradi et al. (2022)** examined the collapse probability and collapse time of a four-story reinforced concrete frame under earthquake and post-earthquake fire loading using ABAQUS and OpenSees. They concluded that increasing peak ground acceleration raised the collapse probability while decreasing the collapse time of the frames. **Lin et al. (2024)** studied concrete-filled steel tubes and concluded that column height significantly influences the inertial response. Higher columns exhibited greater peak inertia effects above the impact point due to the increased mass of the column segment.

**Liu et al. (2024)** studied the impact response of unprotected and protected reinforced concrete beams using aluminum foam and sandwich panels. Their findings indicated that these protective layers effectively shield the beams from damage, altering the failure mode from shear failure to flexure-shear failure. Ulzurrun and Zanuy (2024) characterized the failure modes of reinforced concrete beams under impact loads, observing that the shear-bending path of cross-sections during impact tests follows a distinct bending-to-shear ratio compared to

quasi-static conditions. **Mohammad and Abbas (2023)** investigated the shear strength capacity of dapped-end beams under concentrated loads near supports through experiments, simulations, and mathematical modeling. They proposed a new method to enhance shear strength at the re-entrant corner by incorporating horizontal and hanger steel reinforcement, achieving greater load-carrying capacity compared to conventional methods. Similarly, **Balamuralikrishnan et al. (2023)** studied reinforced concrete beams strengthened with externally bonded spent catalyst-based ferrocement laminates at various percentages (3%, 6%, 9%, and 12%). Strengthened beams showed an 18% increase in flexural capacity, a 16% increase in shear capacity, and a 30% improvement in combined flexural and shear behavior compared to conventional beams. **Hunegnaw et al. (2021)** examined the impact of stirrup orientation on the shear capacity of reinforced concrete beams with varying shear-span-to-depth ratios. Results revealed that inclined stirrup arrangements significantly improved shear capacity compared to conventional vertical arrangements. Additionally, the study highlighted that higher concrete compressive strength enhances shear capacity, emphasizing the role of concrete in shear resistance. **Wang et al. (2024)** noted the importance of designing reinforced concrete beams to fail in a ductile manner, providing warnings before collapse. Under dynamic loading, however, complex cracking patterns emerge that are absent in static conditions. **Slowik (2019)** observed that increasing shear capacity with higher reinforcement ratios is primarily attributed to dowel action, a critical mechanism for shear transfer in heavily reinforced beams. Finally, **Ozbolt et al. (2001)** suggested that advanced models, such as the microplane model with relaxed kinematic constraints, are suitable for analyzing shear crack propagation in reinforced concrete beams. These studies collectively contribute to the understanding and improvement of reinforced concrete structures for safety and engineering applications.

The review of the literature revealed that the influence of concrete strength on under-shear-reinforced concrete beams subjected to impact loading has been inadequately explored. Additionally, the evaluation of the dynamic amplification factor for such beams remains limited. Consequently, this study aims to investigate the behavior of under-shear-reinforced concrete beams under both static and impact loading conditions. The mix proportions, materials, and testing methodology are comprehensively detailed in **Section 2**. The behavior of reduced-scale reinforced concrete beams is analyzed under static and impact loading, as discussed in **Section 3**. A comparative analysis of the performance of these beams under static and impact conditions is conducted, with the dynamic amplification factors calculated and discussed in **Section 4**.

## **2 Materials and methodology**

## 2.1 Cement

The grade of cement used in the study was OPC 43 Grade and the specific gravity of cement is an important property being related to the density and viscosity. The specific gravity of cement largely affects the concrete mix performance and an important parameter for designing the mix for concrete using **IS:10262-2019**. For this reason, the specific gravity test was conducted on the cement. The specific gravity of the cement used is determined with the procedure given in **IS:2720 (Part-III)-1980**. The specific gravity of the cement obtained through the test is 3.15 and the cement used was free from lumps.

## 2.2 Fine aggregates

The fine aggregates used in the experiment were locally available. The fine aggregates should be well graded for proper compaction of concrete and to achieve minimum voids. For this purpose, fine aggregates was tested for sieve analysis in order to determination the particle size distribution of fine aggregates. Sieve analysis test of fine aggregates was conducted as per **IS: 2386 (Part-I) -1963**. Fine Aggregates must also meet the requirements of **IS:383-2016**. The fine aggregates used conforms to grading zone II of Table 4 of **IS:383-2016**. Gradation, moisture content and specific gravity of fine aggregates are important parameters required while designing the concrete mix. The specific gravity of fine aggregates is also determined as per **IS:2386 (Part-III)-1963**. The specific gravity value obtained is 2.6. Water absorption test of fine aggregates was conducted as per **IS:2386 (Part-III)-1963**. The absorbed water percentage was found to be 2.3%.

## 2.3 Coarse aggregates

Locally and easily available coarse aggregates were used in the preparation of concrete. The gradation, specific gravity and moisture content of coarse aggregates are required while designing the concrete mix. The sieve analysis test was conducted on the coarse aggregates as per **IS: 2386 (Part-I) -1963**. Coarse aggregates used conform to Table 2 of **IS:383-2016**. The specific gravity test of coarse aggregates was conducted as per **IS:2386 (Part-III)-1963**. The specific gravity of coarse aggregates is 2.7. The moisture content test on coarse aggregates was conducted using **IS:2386 (Part-III)-1963** found to be 0.5%. The crushed angular coarse aggregates were used. Maximum nominal size of aggregates used is 10mm.

## 2.4 Reinforcement bar

The galvanized steel is used as the reinforcement in the beams. The mechanical test of the galvanized steel was performed using the universal testing machine (UTM) and the tensile strength, yield strength and percentage of elongation are shown in **Table 1**.

**Table 1** Mechanical testing of the galvanised steel

Tensile Strength (N/mm <sup>2</sup> )	Yield Strength (N/mm <sup>2</sup> )	Elongation (%)
875.10	636.44	16.84

## 2.5 Chemical admixture

The concrete of required workability without affecting the water-cement ratio and also the concrete of required strength can be obtained by using superplasticizer. In the present study, Polycarboxylate Ether based superplasticizer was used. The quantity of superplasticizer required for achieving the required slump and required workability was obtained by performing several trial mixes and then the quantity of superplasticizer was obtained.

**Table 2** Concrete mix proportion (by weight)

Concrete Mix	Cement	Fine Aggregates	Coarse Aggregates	Water	Superplasticizer
M50	1	1.9300	1.7307	0.31	0.003
M40	1	1.9187	2.1121	0.26	0.005
M30	1	1.8578	2.1754	0.35	0.0045
M20	1	1.753	1.895	0.40	0.003

## 2.6 Preparation of concrete

The reinforced concrete beam of required strength is achieved through the mix design as per environmental conditions and as per the conditions of aggregates, cement and superplasticizers. The concrete mix designs were performed using **IS:10262-2019**. The mix designs for different grades of concrete were prepared for moderate exposure conditions. As per **IS:456-2000**, Clause 8.2.4.2, the maximum cement content in the concrete mixes is maintained as 450 kg/m<sup>3</sup>. The reinforced concrete beams were casted with four different grades of concrete, viz. M20, M30, M40 and M50. In Indian Continents, the grade of concrete M20 to M55 were used in most of the structural works of ordinary and standard concrete as per **IS 456 :2000**. Therefore, these concrete mixes were considered in the present study.

For all the specimens, 43 grade OPC cement was used and 100 mm slump was maintained for required compaction and ease of work. Once the trial mix is prepared than 150 mm concrete cubes were prepared and were then cured for 28 days and were then tested on the 28<sup>th</sup> day in order to confirm the target strength of prepared mix design. The process is repeated until the

required results achieved. The three different grades of concrete used in present study along with the composition and mix ratio are as shown in **Table 2**.

### 2.7 Neutral axis depth calculation of beams

The relation between the depth of neutral axis and the limiting depth of neutral axis is one of the criteria to identify either the beam section is under-reinforced section or balanced section or over-reinforced section. The formula used for determining the limiting depth of neutral axis ( $X_{u,lim}$ ) is given as  $X_{u,lim} = \frac{700}{(0.87f_y + 1100)}d$ . The actual depth of neutral axis ( $X_u$ ) is determined with the help of the formula as  $0.36f_{ck}bX_u + (f_{sc} - 0.45f_{ck})A_{sc} = 0.87f_yA_{st}$ . The input values are as follows:  $d=75\text{mm}$ ,  $f_t$  is  $875.10\text{ N/mm}^2$ ,  $b$  is  $50\text{ mm}$ ,  $f_y$  is  $636.44\text{ N/mm}^2$ ,  $A_{sc}=A_{st}= 25.133\text{ mm}^2$ . The tension and compression steel ratio was  $0.67\%$ , ( $\frac{A_{st}}{bd}$ ) considered in the present study. The neutral axis depth was calculated considering different grades of concrete are shown in **Table 3**.

**Table 3** Neutral axis depth

Concrete Grade	Depth of confined concrete ( $X_u$ ) from top fibre of the beam in mm	Limiting depth of confined concrete ( $X_{u,lim}$ ) in mm
M20	19.6	31.7
M30	13.1	
M40	9.9	
M50	8.0	

**Table 4** Shear stress values of different grades of concrete as per IS:456-2000

Concrete Grade	Provided shear strength of concrete, $\tau_v$ , ( $\text{N/mm}^2$ )	Required shear strength of concrete, $\tau_c$ , ( $\text{N/mm}^2$ )	Maximum shear strength of concrete, $\tau_{cmax}$ , ( $\text{N/mm}^2$ )
M50	0.17	0.58	4.0
M40		0.58	4.0
M30		0.56	3.5
M20		0.53	2.8

### 2.8 Design of shear reinforcement

The shear strength of the beams was predicted as well as verified with the allowable shear stress in order to design the under shear reinforced beams. The spacing of stirrups considered

in the beam is  $S_v = 50$  mm and  $f_y$  of steel is 636.4 MPa. The cross-sectional area of stirrups is  $A_{sv} = 0.785 \text{ mm}^2$  (for 1 mm diameter bar). The formula for the shear strength,  $V_{us} = 0.87 f_y A_{sv} d / S_v$  from IS:456-2000, Clause 40.4 (a), the value calculated is  $V_{us} = 652$  N. Therefore, the provided shear strength is  $V_{us} / bd$  is  $652 \text{ N} / (50 \times 75 \text{ mm}^2) = 0.17 \text{ N/mm}^2$ . By the method of interpolation, the required design shear strength of concrete is determined. From Table-20 of IS:456-2000, the required shear strength for M20, M30, M40 and M50 grade of concrete is equal to 0.53, 0.56, 0.58 and 0.58  $\text{N/mm}^2$ , respectively. **Table 4** shows shear stress values of different grades of concrete. The required shear stress exceeds the provided shear stress of concrete is rarely occurring human error. Therefore, spacing of stirrups is 50 mm and 1 mm diameter bar was considered in the present study as shown in **Fig. 1(a)** under shear reinforced concrete beam.



**Fig. 1.** (a) Reinforcement mesh and (b) concrete beam specimen

## 2.9 Preparation of specimens

The reduced scale of one-fifth was considered which is equivalent to the cross section of  $0.25 \times 0.5$  m is actual members considering in the range of span of 5 to 5.5m. The chosen beam size ( $50 \times 100$  mm) is practically not feasible however, the size was considered in the present study in order to perform the analysis with shear-deficient members. In addition to that, the selection of beam size for experimental work strictly followed as per IS: 456 considering the deflection limiting criteria of span to depth ration 20 as simply supported beam however, the partial fixed condition was introduced due to the impact loading in the present study. The 4 mm diameter galvanized steel and two numbers at bottom and two numbers at top was used as longitudinal reinforcement in the beam. The 1050 mm long bars were used as longitudinal reinforcement. The centre to centre spacing of stirrups is 50 mm and 1 mm diameter bar 2-legged stirrups were considered. The reinforcement mesh considered in the beam is shown in **Fig. 1(a)**. The beam specimens were prepared and 3 cubes also prepared during casting of beams in order to determine the compressive strength of the concrete. The calculated quantity of materials is first dry mixed in the mixer and after that water and superplasticizers are added. The slump was maintained during casting of beams 100 mm. The reinforcement mesh is then

placed in the mould and then centered so as to maintain the required clear cover. The concrete was poured after achieving proper consistency of mixes. The specimen was then allowed to dry for 24 hours and then demoulded and the specimen after demould is shown in **Fig. 1(b)**. The specimens were cured for 28 days immediately after demoulding. After 28 days, the specimens and cubes were allowed to surface dry for 1 day and then the cubes were tested to measure the compressive strength of the concrete, while the beams are whitewashed through which the cracks can be easily identified during testing.

### **3 Experimental program**

#### **3.1 Three point impact test**

The impact strength of concrete was studied in terms of impact force versus time and the deformed profile of the concrete are discussed in this section. The strength of the concrete was varied as 20, 30, 40 and 50 MPa against the mix M20, M30, M40 and M50, respectively. Beam is placed on the bottom rigid support. In order to restrict the lateral movement of beams in any direction, the beam is clamped with the help of hollow iron rods using nuts and bolts. To study the effect of impact energy on the resistance of beams under impact loading, a 60° angle of impact was considered. Beam specimens were tested using a swinging pendulum drop-weight system, as illustrated in **Fig. 2(a)**. The machine has a maximum weight capacity of 90 kg and a maximum drop height of 3.47 m, corresponding to a 135° angle of impact. The pendulum's angular guided motion ensured precise impact at the center of the specimens. The system comprises six circular steel pipe sections with a diameter of 50.4 mm and two C-channel steel sections (100 × 50 × 5 mm), all securely bolted with 10 mm diameter bolts. The supports were spaced 900 mm apart, and the impactor, featuring a 90 mm diameter hemispherical nose, was attached to a solid steel section with three additional weights, each weighing 15 kg, bringing the total weight to 60 kg. The hemispherical nose was found to provide conservative results for reduced-scale reinforced concrete beams. A load cell mounted between the impactor and the solid section ensured rigidity and minimized energy loss during impact. The pendulum was operated using a steel coil connected to a release mechanism, and rubber pads were installed to prevent collisions with the apparatus. The pancake-type dynamic load cell, capable of measuring impact forces up to 250 kN with a resonant frequency of 8.7 kHz, was used to capture data. The load cell's data were recorded at a sampling rate of 50 kHz via a DNA-AI-211 data acquisition system, which has a maximum sampling rate of 100 kHz. The impact angle was adjusted with an angle setter, and at 60°, the impact velocity reached 5.182 m/s. The load cell's placement played a crucial role in accurately measuring impact forces, particularly for hemispherical impactors. According to **Li et al. (2020)**, the mass distribution of the drop weight

can influence force measurements when the load cell is positioned between the impactor head and the trailing weight. To address this, a mass ratio factor ( $\alpha$ ) was introduced, defined as the ratio of the mass of the weight above the load cell ( $m_w$ ) to the mass of the impactor head ( $m_h$ ). The test facility for impact loading is depicted in **Fig. 3**. A mass ratio of less than 20 requires correction factor  $\beta_c = (1 + 1/\alpha)$  to be multiplied to the measured impact force to get correct values of impact force-time plot. In this study, the value of  $\alpha$  was found to be  $\alpha = 2.9/60 = 20.68$ , therefore no correction to the impact force was applied.

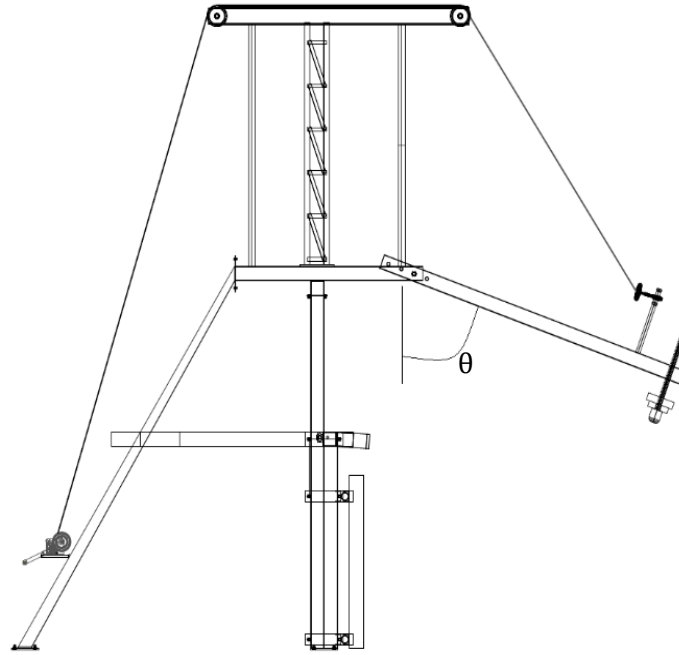


**Fig. 2.** (a) Swinging pendulum drop impact test machine schematic at 60° impact



**Fig. 3.** (a) Testing frame (b) Impactor with load cell and (c) beam after impact

Further, the force time curve revealed that the time at which impact force attained peak values were found to be same for chosen cases. The first peak load obtained as a result of a impact load on RC beam of M20, M30, M40 and M50 concrete are 28, 35, 46 and 60 kN,

respectively, **Fig. 4**. After the first rise, the load does not become zero instantly and longitudinal stress wave led to second peak. The second peak force of M20, M30, M40 and M50 concrete are 11.5, 15.7, 16 and 21.8 kN, respectively. However, third peak force was found to be almost same in the range of 8-12 kN for the chosen cases. It was also observed that the three peaks were found to be within 0.002 sec. duration. It was concluded that there is no direct relationship between impact velocity and time of peak force, however, peak force tends to increase with increase of concrete compressive and tensile strength.

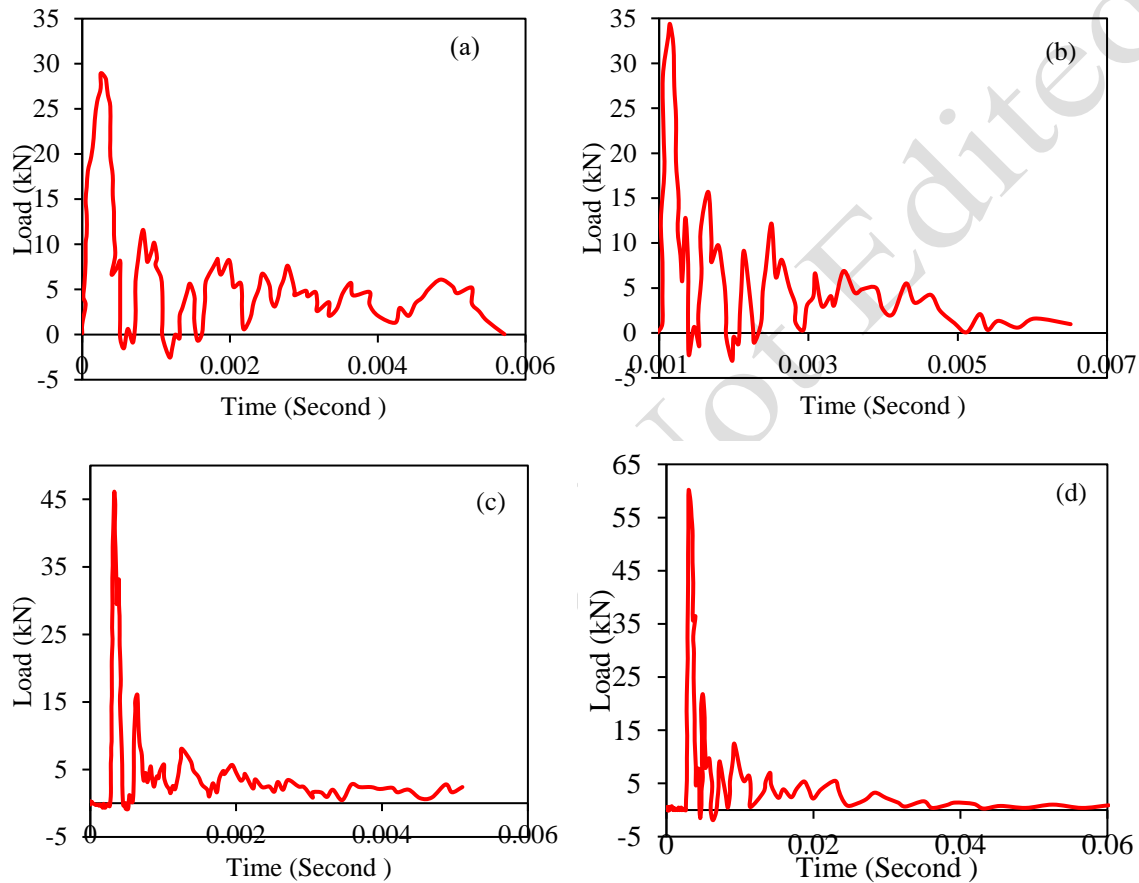


**Fig. 3.** Response of (a) M20 (b) M30 (c) M40 and (d) M50 concrete beam under impact loading

As a result of impact, cracks spread from the center of the beam to the side faces of the beam along the horizontal direction of the beam, see **Fig. 4**. It should be noted that the cracks were in close vicinity of the impact point and marginal flexural failures. It was observed that the single however, significantly wide cracks at the tension face were developed for the chosen cases. However, the couple of flexural cracks at the tension face were developed in case of M50 concrete. The failure pattern of results may be attributed to the reason that shear stress value of the beam is much less than the required shear stress that can be sustained by concrete. It was also observed that the jerk induces and travels through the thickness of the beam, which

is so large that the reinforcement on the tension side of the beam breaks apart into two. Failure pattern of the beams also witnessed as the required shear strength is in the range of 0.53 to 0.58 MPa whereas the provided shear strength is 0.17 MPa.

(a)



(b)



(c)





**Fig. 4.** Crack pattern of (a) M20 (b) M30 (c) M40 and (d) M50 concrete beam after impact

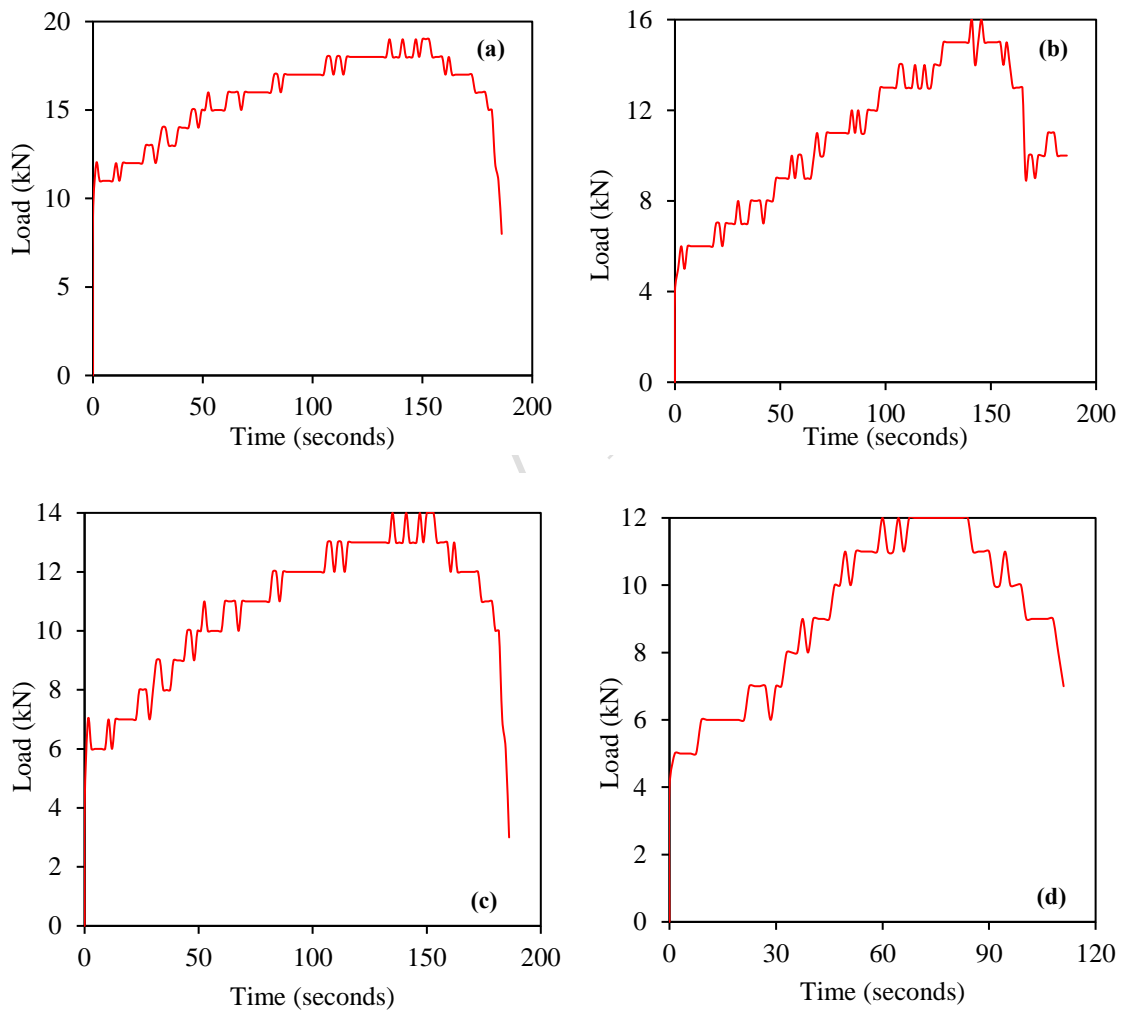


**Fig. 5.** Response of (a) M50 (b) M40 (c) M30 and (d) M20 concrete beam under four-point bending test

### 3.2 Four-point static tests

In order to assess the influence of strength of concrete under impact loading, a benchmark study was performed under static loading. Therefore, the four-point loading test under UTM was performed is discussed in this Section and the force versus time results were

converted theoretically into three-point static tests is discussed in the next Section. The equipment firstly was set up for compression space. An adjustable crosshead was brought down to hold the loading plate. Then the spacing between the roller supports was fixed at 900 mm. After that, the beam was set up on the rollers and the spacing on both sides of the rollers was set. Then the upper Jaw was placed on the beam at the centre of the beam. The set up for four-point bending test is shown in **Fig. 5**. The peak load values obtained as a result of a four-point bending test of RC beams for M20, M30, M40 and M50 Grades are 19, 16, 14 and 12 kN, respectively. The load versus time history was also obtained through these tests and the peak load was also recorded.



**Fig. 6.** Reinforced concrete beam of (a) M20 (b) M30 (c) M40 and (d) M50 concrete grades (i) before and (ii) after the four-point bending test

**Fig 6** illustrates the crack patterns observed in eight beams of M20, M30, M40, and M50 concrete grades, tested under static loading with two repetitions for each grade. As the load increased, cracks progressively formed on both faces of the beams. Generally, low-strength concrete beams exhibited brittle failure with rapid crack propagation, while medium-strength

concrete beams typically failed in a ductile manner, characterized by slower crack growth. However, in the present study, all reinforced concrete beams, regardless of strength grade, failed in a brittle manner with rapid crack propagation due to the absence of shear reinforcement, as shown in **Fig. 6(a-ii to d-ii)**. Deformation beneath the loading point continued to increase until the beams ultimately failed. These findings are consistent with those of **Ahmad et al. (1995)**, who noted that in beams with limited shear reinforcement, the shear ductility index decreases as concrete strength increases. Similarly, **Slowik (2019)** observed that highly reinforced concrete beams lacking transverse reinforcement are prone to brittle failure caused by shear and diagonal cracks. The irregular failure patterns across varying concrete grades can be attributed to reduced shear ductility as concrete strength increases. This reduction, coupled with high shear forces and the development of diagonal cracks, leads to brittle failure in reinforced concrete beams.

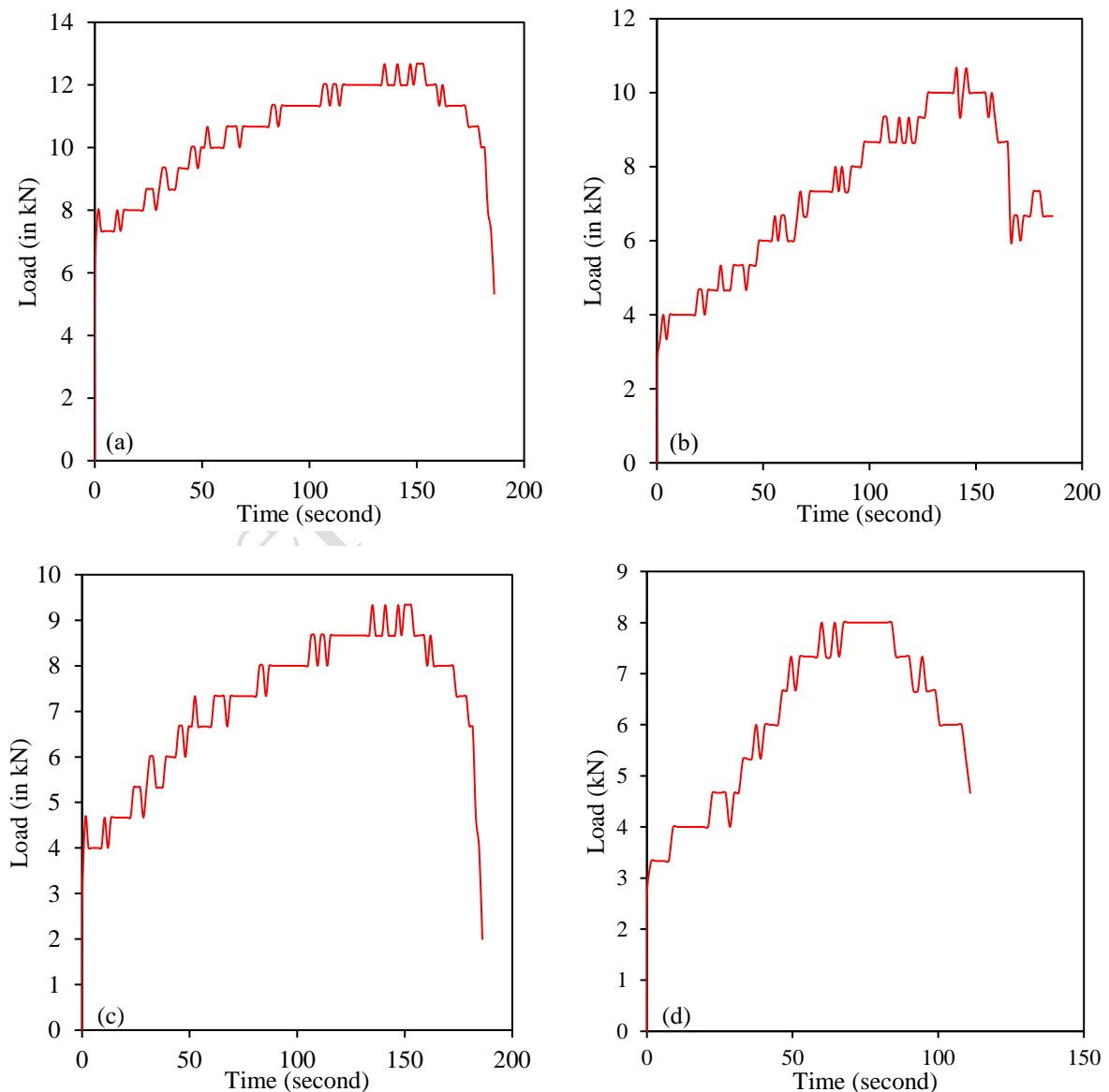


**Fig. 7.** Response of (a) M50 (b) M40 (c) M30 and (d) M20 concrete beam under three-point bending test

### 3.3 Conversion of four point bending results into three point bending results

The four-point loading test was performed and the results were converted into the three-point loading in order to keep the test configuration equivalent to impact loading as a three-point impact load test. The specific assumptions were taken into consideration when converting three-point bending from four-point bending is that the beam material is linear elastic, which means that Hooke's Law applies. This suggests that strain and stress are closely correlated, and that after unloading, the material will elastic. According to the concept, the beam's deformations (deflections) are minimal in comparison to its size. This makes it possible to use linear approximations in the bending equations. In order to make the computation of moments of inertia and other attributes easier, it is common practice to assume that the beam has a constant cross-section throughout its length. The flexural strength formulae by three-point bending method and four-point bending method were equated in order to convert the four-point bending data into three-point bending data. The formula for flexural strength by four-point bending tests is  $f_b = Pl/bd^2$ , whereas the same for three-point bending tests is  $f = 3Fl/2bd^2$ . Further, all loads corresponding to three-point bending were obtained and the load versus time history obtained as a result of calculation are as shown in **Fig. 7**.

The maximum forces measured from the four-point and three-point bending tests for concrete grades M50, M40, M30, and M20 are summarized in **Table 5**. For the three-point bending test, the peak forces were recorded as 12.67, 10.67, 9.33 and 8 kN for M50, M40, M30, and M20 grades, respectively. In contrast, the peak forces for the four-point bending test were significantly higher, measured at 19, 16, 14 and 12 kN for the same grades. The overall difference in the maximum forces between the two testing methods was approximately 33%, indicating a substantial variance in load distribution and force measurement outcomes between the two approaches. The differences in the test results can be attributed to the load application mechanisms inherent to each method. In the three-point bending test, the load is applied at a single point, creating a localized stress concentration and resulting in a lower overall force measurement. On the other hand, the four-point bending test applies the load over two points, distributing the stresses more uniformly along the beam and allowing for higher force measurement before failure. This difference in loading conditions can influence the measured material properties, particularly the modulus of elasticity and the modulus of rupture. In terms of accuracy, it has been reported by **Brancheriau et al. (2002)** that the three-point bending test underestimates the modulus of elasticity by approximately 19% when compared to the four-

point bending test. This discrepancy arises due to the localized nature of the stress field in the three-point bending test, which does not capture the material's full deformation response. Moreover, **Mujika et al. (2016)** highlighted that horizontal forces are more critical in four-point bending tests, as these forces better simulate real-world bending scenarios, resulting in more reliable and representative data for structural applications. **Paulo and Brancheriau (2018)** further observed that the modulus of rupture obtained from three-point bending tests was about 5.2% higher than that from four-point bending tests in studies on Eucalyptus wood specimens. This suggests that while the three-point bending test may provide slightly higher rupture values due to the focused stress concentration, it may not fully represent the material's behavior under distributed loads.

**Table 5.** Comparison of four point and three point bending tests results

Concrete Strength	Four Point Bending Result (kN)	Three Point Bending Result (kN)	Percentage difference
M50	19	12.67	33.333
M40	16	10.67	
M30	14	9.33	
M20	12	8.00	

#### 4. Results and discussion

The bending resistance of under shear reinforced concrete beam with varying strength was measured under static and impact loading are compared in this section. Also, the dynamic factor of under shear reinforced concrete beam with varying strength was calculated and discussed in this Section.

##### 4.1 Comparison of static and impact tests results

The results obtained for the peak loads of M20, M30, M40, and M50 grade concrete beams under impact loading were significantly higher than those measured in the three-point bending tests. Specifically, the peak loads for impact loading were 28, 35, 46 and 60 kN, while the corresponding values from the three-point bending tests were 8, 9.33, 10.67 and 12.67 kN, respectively. This discrepancy between static and dynamic loading highlights how concrete's structural behavior can vary drastically under different loading conditions. Both static and impact strength increase with the strength of the concrete, which is to be expected, but the deformed profile of the beams is notably influenced by the lack of confined shear reinforcement, a factor that significantly affects the failure modes and crack propagation

behavior of the beams under impact. The reason for this heightened performance under impact loading can be attributed to strain rate sensitivity, which describes how materials respond differently when loads are applied at varying rates. The behavior of concrete under impact loading can be explained by combining the classical Griffith theory of fracture mechanics with the concept of sub-critical crack growth. Griffith's theory postulates that brittle materials fail when the size of a flaw exceeds a critical threshold for a given stress level. The theory uses an energy balance approach, suggesting that the energy spent in crack propagation is equal to the energy required to create new crack surfaces. According to Griffith, the fracture strength of a material with an existing flaw is inversely proportional to the square root of the crack size, meaning that larger cracks lead to weaker materials that fail under lower stress. Moreover, the fracture strength is proportional to the square root of the surface energy, implying that materials with higher surface energy require more work to propagate cracks, making them more resistant to failure. An important aspect of this theory is that materials with smaller cracks require more strain energy to propagate those cracks, and thus, they demonstrate better resistance to failure. However, the effect of sub-critical crack growth further explains the differing behavior under static and dynamic loading. Under sustained static loading, flaws in a material can grow incrementally over time, eventually reaching a critical size that causes failure. This process is relatively slow, giving the flaws ample time to grow, and consequently, failure occurs at a lower load level. In contrast, under impact loading, the load is applied very rapidly, leaving little to no time for these sub-critical cracks to grow. As a result, the material can endure higher stresses before failure occurs, because the growth of critical flaws is prevented or delayed by the fast rate of loading. This explains why the peak loads observed under impact conditions are significantly higher than those observed under static loading. The higher rate of load application allows the beams to sustain more force before failure, despite the presence of flaws or cracks. However, this also means that under static loading, where cracks have time to grow, the failure occurs at lower load levels. Furthermore, the lack of shear reinforcement contributes to the brittle failure mode, especially under higher-strength concrete grades where the increased shear forces and diagonal cracks lead to more rapid failure.

The deformation of the reinforced concrete beam found failed by shear due to the lack of confined shear reinforcement. Failure pattern of the beams also witnessed as the required shear strength is in the range of 0.53 to 0.58 MPa whereas the provided shear strength is 0.17 MPa. In addition to that, the depth confined concrete was measured and shown in **Table 3** and the confined concrete depth is directly related to the shear resistance of the concrete. The confined concrete depth is 19.6, 13.1, 9.9 and 8 mm corresponding M20, M30, M40 and M50 grade

concrete whereas the limiting confined depth is 31.7 mm. The deformation in the beam is led by shear failure and no flexural failures were developed on the beam under both static and impact loading.

#### 4.2. Dynamic amplification factor

The Dynamic Amplification Factor (DAF) is traditionally defined as the ratio of dynamic strength to static strength. This ratio is widely used to quantify the effects of strain rate. In this study, the DAF is calculated as the ratio of  $P_d/P_s$ , where  $P_d$  represents the generalized deforming force (calculated by excluding the inertial force from the total force), and  $P_s$  is the peak static bending capacity of the specimen. However, generalized deforming force is considered as peak force in the present study and the inertial force of the beams couldn't calculate due to the non-availability of acceleration results. The dynamic amplification factor for the chosen cases is calculated and shown in **Table 6**. It was observed that the dynamic amplification factor increases with increase of concrete strength and highest DAF found to be 4.75 corresponding M50 concrete strength whereas same was found to be 3.5 corresponding M20 concrete strength and similar results were observed by **Parida et. al. (2020)**. It was stated that the DAF is not uniform in each member of the truss girder bridge and they concluded that the drawback in codal formulae for the impact factor in bridge design. It is to note that the **Parida et. al. (2020)** considered yield load which was obtained from the linear static analysis to measure the DAF whereas the peak load (ultimate load) was considered in the present study which is useful to define the large deformation problems and the design of bridges and barriers etc. It is also to be noted that the dynamic amplification factor is maximum 1.5 as per **IS 1893:2016**. The relation between the DAF and compressive strength of concrete was multifaceted and found to affect the structural safety and design. It is suggested engineers to understand this relationship in order to take decisions about material selection, design strategies, and compliance with building codes, ultimately enhancing the resilience and reliability of structures under dynamic loading conditions. Further, medium strength concrete exhibit different cracking patterns and failure mechanisms under dynamic loading, which can influence the DAF.

**Table 6.** Dynamic amplification factor

Concrete Strength	Dynamic ultimate load $P_d$ (kN)	Static ultimate load $P_s$ (kN)	Dynamic amplification factor
M50	60	12.67	4.75
M40	46	10.67	4.30
M30	35	9.33	3.75

## 5. Conclusions

The influence of concrete strength on under shear reinforced concrete beams against static and impact loading was studied. The strength of the concrete was varied as 20, 30, 40 and 50 MPa considering the conventional concrete widely used in the Civil Engineering applications. The results were presented and discussed in terms of impact force and deformed profile. Further, the dynamic increase factor was calculated and the following conclusions were drawn:

- It was observed that the resistance of beams increased with the strength of concrete under both static and impact loading. Additionally, the peak static force measured in four-point bending tests was found to be 33% higher than that in three-point bending tests.
- The resistance of beams under impact loading was found to increase significantly compared to static loading. This can be attributed to strain rate sensitivity, which can be explained by combining the classical Griffith theory with the concept of sub-critical crack growth. According to the Griffith theory, failure in brittle materials occurs when a flaw reaches a critical size for a given stress level.
- The deformation of reinforced concrete beam is purely by shear failure and the reason may be due to the lack of shear capacity of the beams. It was also observed that providing lesser shear reinforcement causes brittle failure of the concrete. It was concluded that the under shear reinforcement changes the course of results under static conditions. The study indicates that the shear reinforcement is very important for structure in order to ensure a ductile failure rather than the concrete strength. The grade of concrete strength may not be a matter if insufficient shear reinforcement was used in the design.
- The dynamic increase factor increases with increase of concrete strength and highest DAF found to be 4.75 corresponding M50 concrete strength whereas same was found to be 3.5 corresponding M20 concrete strength. In light of structural designer's point of view, the DAF of the member with M50 concrete proposed in the present study is 4.75 and this member will carry a failure load of 4750 kN under impact load irrespective of bridge and crash barrier if the beam is designed for 1000 kN capacity under static condition.

## References

1. Anike, E.E., Saidani, M., Olubanwo, A.O. and Anya, U.C. (2022). "Flexural performance of reinforced concrete beams with recycled aggregates and steel fibres", *Structures*, 39, 1264-1278, <https://doi.org/10.1016/j.istruc.2022.03.089>.
2. Anil, O., Durucan, C., Erdem, R.T. and Yorgancilar, M.A. (2016). "Experimental and numerical investigation of reinforced concrete beams with variable material properties under impact loading", *Construction and Building Materials*, 125, 94-104, DOI: 10.1016/j.conbuildmat.2016.08.028.
3. Ahmad, S.H., Xie, Y. and Yu, T. (1995). "Shear ductility of reinforced concrete beams of normal and high-strength concrete", *Cement and Concrete Composites*, 17(2), 147-159, [https://doi.org/10.1016/0958-9465\(94\)00029-X](https://doi.org/10.1016/0958-9465(94)00029-X).
4. Banthia, N.P., Mindess, S. and Bentur, A. (1987). "Impact behaviour of concrete beams", *Journal of Materials and Structures*, 20, 293-302, DOI: 10.1007/BF02485926.
5. Bhatti, A.Q. and Kishi, N. (2011). "An application of impact-response analysis on small-scale RC arch-type beams without stirrups", *Construction and Building Materials*, 25, 3972-3976, DOI: 10.1016/j.conbuildmat.2011.04.030.
6. Balamuralikrishnan, R., Al-Mawaali, A.S.H., Al-Yaarubi, M.Y.Y., Al-Mukhaini, B.B. and Kaleem, A. (2023). "Seismic upgradation of RC beams strengthened with externally bonded spent catalyst based ferrocement laminates", *High Tech and Innovation Journal*, 4, (1), 189-209, <http://dx.doi.org/10.28991/HIJ-2023-04-01-013>
7. Brancheriau, L., Bailleres, H. and Guitard, D. (2002). "Comparison between modulus of elasticity values calculated using 3 and 4 point bending tests on wooden samples", *Wood Science and Technology*, 36, 367–383.
8. El-Mandouh, M.A. and Abd El-Maula, A.S. (2021). "Shear strength of epoxy-modified reinforced concrete beams", *Innovative Infrastructure Solutions*, 6, 105, doi:10.1007/s41062-021-00483-3.
9. Fang, Y., Min, W., Dali, Y. and Weichuang, Y. (2022). "Study on flexural behavior of self-compacting concrete beams with recycled aggregates", *Buildings*, 2022, 12(7), 881, <https://doi.org/10.3390/buildings12070881>.
10. Fujikake, K., Li, B. and Soeun, S. (2009). "Impact response of reinforced concrete beam and its analytical evaluation", *Journal of structural engineering*, 135, 938-950, DOI: 10.1061/(ASCE)ST.1943-541X.0000039.
11. Hunegnaw, C. and Aure W. T. (2021) "Effect of orientation of stirrups in combination with shear span to depth ratio on shear capacity of RC beams", *Heliyon*, 7(10), <https://doi.org/10.1016/j.heliyon.2021.e08193>

12. Indian Standard 1893:2016, Part 1 Criteria for earthquake resistant design of structures, *Bureau of Indian Standards*, New Delhi.
13. Indian Standard 10262-2019, Concrete mix proportioning-guidelines, *Bureau of Indian Standards*, New Delhi.
14. Indian Standard 2720-Part-III-1980, Method of tests for soil Part-III, Determination of specific gravity, Section-II Fine, Medium and Coarse Grained Soils, *Bureau of Indian Standards*, New Delhi.
15. Indian Standard 2386-1 (1963), Methods of test for aggregates for concrete, Part I: Particle Size and Shape, *Bureau of Indian Standards*, New Delhi.
16. Indian Standard Code, IS:383-2016, Coarse and fine aggregate for concrete – specification, *Bureau of Indian Standards*, New Delhi.
17. Indian Standard 2386-3 (1963), Methods of test for aggregates for concrete, Part 3: Specific gravity, density, voids, absorption and bulking, *Bureau of Indian Standards*, New Delhi.
18. Indian Standard Code 456 (2000), Plain and reinforced concrete - code of practice, *Bureau of Indian Standards*, New Delhi.
19. Jin, L., Renbo Z., Xiuli D. and Guoqin D. 2020. "Structural behavior of the steel fiber reinforced concrete beam under multiple impact loadings, An Experimental investigation", *International Journal of Damage Mechanics*, 29(3), 503–26, DOI: 10.1177/1056789519862331.
20. Li, H., Chen, W. and Hao, H. (2020). "Factors influencing impact force profile and measurement accuracy in drop weight impact tests", *International Journal of Impact Engineering*, 145, 103688, <https://doi.org/10.1016/j.ijimpeng.2020.103688>.
21. Lin. S., Zhang, B., Zhang, S., Zhang, Y. and Hu, X. (2024). "Dynamic responses of concrete-filled steel tubes impacted horizontally by a rigid vehicle: Experimental study and numerical modelling", 199, 111826, <https://doi.org/10.1016/j.tws.2024.111826>.
22. Liu, K., Cheng-Qiang, G., Yuan, J., Jie-Xin, D. and Shao-Bo, K. (2024). "Experimental and numerical investigations on impact response of reinforced concrete beams with a sandwich panel protective layer", *Engineering Structures*, 316, 118543, <https://doi.org/10.1016/j.engstruct.2024.118543>.
23. Meola, C., Boccardi, S. and Carlomagno, G.M. (2018). "Infrared thermography for inline monitoring of glass/epoxy under impact and quasi-static bending", *Applied Sciences*, 8(2), 301, <https://doi.org/10.3390/app8020301>.

24. Mohammad, A.K. and Abbas, R.M. (2023). "Interaction strength of hanger and horizontal steel reinforcement of dapped end beams", *Civil Engineering Journal*, 9(12), 3174-3185, <http://dx.doi.org/10.28991/CEJ-2023-09-12-015>.
25. Moradi, M., Tavakoli, H.R and Abdollahzade, GH.R. (2022). Collapse probability assessment of a 4-story RC frame under post earthquake fire scenario, *Civil Engineering Infrastructures Journal*, 55(1), 121-137, DOI: 10.22059/CEIJ.2021.313241.1718.
26. Mujika, F., Arrese, A., Adarraga, I. and Oses, U. (2016). "New correction terms concerning three-point and four-point bending tests", *Polymer Testing*, 55, 25-37, <https://doi.org/10.1016/j.polymertesting.2016.07.025>.
27. Ozbolt, J., Li, Y., Kozar, I. (2001). "Microplane model for concrete with relaxed kinematic constraint", *International Journal of Solids and Structures*, 38(16), 2683–2711, [https://doi.org/10.1016/S0020-7683\(00\)00177-3](https://doi.org/10.1016/S0020-7683(00)00177-3).
28. Parida, S. and Talukdar, S. (2020). "An insight to the dynamic amplification factor for steel truss girder bridge", *International Journal of Steel Structures*, 20, 1341-1354, doi:10.1007/s13296-020-00364-y.
29. Paulo, R.G.H. and Brancheriau, L. (2018). "Comparison between three-point and four-point flexural tests to determine wood strength of eucalyptus specimens", *Maderas Ciencia y tecnología*, 20(3), 333 - 342, <http://dx.doi.org/10.4067/S0718-221X2018005003401>.
30. Saifullah, I., Nasir-uz-zaman, M., Uddin, S.M.K., Hossain, M.A. and Rashid, M.H. (2011). "Experimental and analytical investigation of flexural behavior of reinforced concrete", *International Journal of Engineering & Technology*, 11, 146-153, DOI: 11 8101 4747 ijet-ijens.
31. Sindy. S.P., González-Fonteboa. B., Martínez-Abella. F. and Eiras-López. J. (2018). "Flexural performance of reinforced concrete beams made with recycled concrete coarse aggregate", *Engineering Structures*, 156, 32-45, <https://doi.org/10.1016/j.engstruct.2017.11.015>.
32. Słowik, M. (2019). "The analysis of failure in concrete and reinforced concrete beams with different reinforcement ratio", *Archive of Applied Mechanics*, 89(5), 885-895. DOI: 10.1007/s00419-018-1476-5.
33. Soleimani, S.M. and Sajjad S.R. (2019). "Analytical study of reinforced concrete beams tested under quasi-static and impact loadings", *Applied Sciences*, 9(14), 2838, <https://doi.org/10.3390/app9142838>.

34. Ulzurrun, G.S.D. and Zanuy, C. (2024). "Dynamic shear force-bending moment interaction diagrams in RC beams under impact", *Engineering Structures*, 308, 118021, <https://doi.org/10.1016/j.engstruct.2024.118021>.
35. Wadhah, M., Ali, T.K.M., Al-Kumzari, Y., Al-Hosni M., Al-Fazari, K. and Al-Bashkardi, M. (2021). "Flexural performance of reinforced concrete beams made by using recycled block aggregates and fibers", *Innovative Infrastructure Solutions*, 6(1), 13. doi:10.1007/s41062-020-00402-y.
36. Wang, H., He, X., Zhou, M., Wu, C., He, J. (2024) "Study on bending failure and crack characteristics in ductile fiber-reinforced concrete beams", *Structural Concrete*. 25:916–934. Doi: 10.1002/suco.202300530.
37. Wongmatar, P., Hansapinyo, C., Vimonsatit, V. and Chen, W. (2018). "Recommendations for designing reinforced concrete beams against low velocity impact loads", *International Journal of Structural Stability and Dynamics*, 18, 1850104, DOI: 10.1142/S0219455418501043.
38. Wu, M., Chen, Z. and Zhang, C. (2015). "Determining the impact behavior of concrete beams through experimental testing and meso-scale simulation: I. Drop-weight tests", *Journal of Engineering Fracture Mechanics*, 135, 94-112, DOI: 10.1016/j.engfracmech.2014.12.019.
39. Zhou, K.J.H., Ho, J.C.M. and Su, R.K.L. (2011). "Flexural strength and deformability design of reinforced concrete beams", *Procedia Engineering*, 14 1399–1407, doi:10.1016/j.proeng.2011.07.176